Journal of Applied Spectroscopy, Vol. 80, No. 3, July, 2013 (Russian Original Vol. 80, No. 3, May–June, 2013)

CHARACTERIZATION OF SEMICONDUCTOR DEVICES AND WAFER MATERIALS VIA SUB-NANOSECOND TIME-CORRELATED SINGLE-PHOTON COUNTING

**V. Buschmann,[a] H. Hempel,[b] A. Knigge,[c]
C. Kraft,[b] M. Roczen,[d] M. Weyers,[c]
T. Siebert,[a] and F. Koberling[a]**

UDC 621.315.592

Time-correlated single-photon counting (TCSPC) of semiconductor photoluminescence is presented as a versatile technique for addressing diverse aspects of charge carrier dynamics on a pico- to microsecond time-scale. Particularly, advantages of expanding this time-domain technique with spectral and spatial resolution are demonstrated. By differentiating the spectral channels within the photoluminescence signal, dynamics of the charge carriers can be correlated to particular materials and substructures for analyzing their functions in complex, multi-component systems. Diffusion and transport phenomena become directly accessible, and localized variations of charge carrier lifetimes can be associated with a particular morphology when the measurements are carried out in the context of microscopic imaging. These general capabilities are demonstrated specifically on a GaAsP quantum well embedded both in an AlGaAs layer structure and in a multi-layer CdTe-CdS heterojunction system.

Keywords: *semiconductor devices, sub-nanosecond time correlation, single photon, time-resolved photoluminescence (TRPL), sub-nanosecond time correlated single photon counting (TCSPC).*

Introduction. The type of charge carrier dynamics in semiconductors is determined by the architecture and function of a respective device and directly reflects the nature and quality of wafer materials [1–3]. This makes precise and efficient measurement techniques of the free charge carrier lifetime essential for characterizing these systems. For a particular class of semiconductors, the characteristic charge carrier lifetime is highly dependent on the nature and dimensions of the materials and interfaces involved. Surface effects, passivation, and the energy transfer efficiency of sensitizers as well as the presence of dopants, impurities, and defect sites can introduce significant variations in this parameter [4–13]. Since the photoluminescence of semiconductors is a direct monitor of the charge carrier dynamics, the general methodology of time-resolved photoluminescence (TRPL) via time-correlated single photon counting (TCSPC) and peripheral technology is highly suited for analysis of phenomena that determine fast charge carrier dynamics in a semiconductor [2, 3, 14]. The technique relies on picosecond pulsed laser excitation that generates charge carriers within a short time window in a localized region of the material at moderate to high injection levels. By subsequently monitoring the statistics of the emission times of photoluminescence after photo-excitation with fast single photon avalanche diodes (SPADs), the mechanism for the charge carrier dynamics in a particular system can be characterized down to the sub-nanosecond time scale.

Parameters of different semiconductor materials, which are relevant for a characterization with TRPL via TCSPC, are summarized in Table 1. From this overview, it can be seen that this general approach is particularly suited for fast charge carrier dynamics. This includes the time scale associated with common III–V and II–VI direct semiconductors in the nanosecond regime as well as the somewhat slower dynamics of the more complex I–III–VI_2 CIGS, organic and dye sensitized systems that span nano- to microsecond domains [1, 4, 5, 7–11, 15–24]. For the case of indirect silicon-based systems, the approach of TRPL can be differentiated from other techniques employed to analyze semiconductors. TRPL offers the unique advantage of directly monitoring fast charge carrier dynamics via the optical emission from the material.

[*]To whom correspondence should be addressed.

[a]PicoQuant GmbH, Rudower Chaussee 29, 12489 Berlin, Germany; e-mail: buschmann@picoquant.com; [b]Institut für Festkörperphysik, Friedrich Schiller Universität Jena, Germany; [c]Ferdinand Braun Institut, Leibniz Institut für Höchstfrequenztechnik, Berlin, Germany; [d]Helmholtz Zentrum Berlin für Materialien und Energie, Institut für Silizium Photovoltaik, Berlin, Germany. Published in Zhurnal Prikladnoi Spektroskopii, Vol. 80, No. 3, pp. 459–467, May–June, 2013. Original article submitted October 30, 2012.

0021-9037/13/8003-0449 ©2013 Springer Science+Business Media New York

TABLE 1. Semiconductor Materials and Characteristic Parameters

Material and literature	Lifetime range	Band gap
GaAs [1, 4, 15–19]	ns	1.42 eV (873 nm)
CdTe[1, 5, 20–22]	ns	1.50 eV (823 nm)
CIGS [7, 8]	ns–μs	1–1.7 eV (1240–729 nm)
Dye Sensitized Solar Cell (DSSC)	ns–μs	visible and NIR regime
Organic [9–11]	ns–μs	visible and NIR regime
Si [1, 23, 24]	μs–ms*	1.12 eV (1100 nm)

*Not suited for TRPL except for special cases such as silicon nanodots [23, 24].

TABLE 2. Picosecond Diode Laser Sources

Diode laser (PicoQuant)	Wavelength, nm	Average power at 40 MHz, mW	Pulse duration, ps	Repetition rate
LDH-P-C-440	440	0.3 1.0	< 90 < 300	32 kHz to 40 MHz
LDH-P-FA-595	595	> 0.3	< 130	10 kHz to 40 MHz
LDH-P-C-635B	635	0.3 4.5	< 100 < 400	32 kHz to 80 MHz
LDH-P-810	810	0.4 5.0	< 90 < 500	32 kHz to 80 MHz

In comparison, longer (micro- to millisecond) time scales are more readily accessible with techniques that utilize other measurement parameters such as photo-conductance to access the types of charge carrier dynamics. In this regime, quasi-steady-state photo-conductance (QSSPC) and microwave detected photo-conductance decay measurements (μPCD) are well established techniques to characterize silicon-based systems. By contrast, TRPL via single photon counting offers a variety of additional advantages in the regime of faster time scales that are inaccessible with other techniques.

Below, an overview of the capabilities available to the general TRPL–TCSPC methodology is presented when the instrumentation of this time-domain technique is expanded to allow for spectral and spatial resolution. This allows for correlating specific dynamic aspects of charge carriers with material characteristic emission channels and the spatial mapping of selected regions of the system. With this multi-dimensional approach, a versatile and powerful methodology for addressing current topics in semiconductor research and design becomes available. The exemplary measurements will focus on a GaAsP quantum well system embedded in a multilayer stack as used in high-power laser diodes [15–19]. The central aim is a clear differentiation of the charge carrier lifetimes in individual layers, which is crucial to the function of these systems. Furthermore, thin layer CdTe–CdS heterojunction systems are characterized in view of the enhanced efficiencies resulting from morphological changes and modifications in material composition due to post-deposition chemical treatment [21–23].

Methodology. Central to resolving charge carrier lifetimes on the sub–nanosecond time scale via TRPL measurements is the combination of pulsed diode laser sources that offer picosecond excitation over the relevant spectral regions of common semiconductor materials and fast single photon detectors that match the time resolution of pulsed illumination in the detection of the single photon emission statistics. Table 2 gives an overview of the picosecond diode lasers employed in this study. These sources generally offer excitation with sub-100 ps (FWHM) pulses within the characteristic regime of band gap transitions typical of III–V and II–VI semiconductor materials as well as I–III–VI_2 CIGS and organic systems. For maximum

TABLE 3. Single Photon Counting Detectors

Detector	Time resolution IRF* (FWHM), ps	Maximum Detection Efficiency, %
PDM-1CTC (Mirco Photon Devices)	100	49 (550 nm)
PMA-192 (PicoQuant)	220	20 (470 nm)
SPD-A-M1 (Aurea Technologies)	260	27 (1200 nm)
τ-SPAD (PicoQuant)	370	75 (670 nm)

*Measured with pulsed diode laser excitation. The values contain the contributions from the complete measurement system, including detector, diode laser and photon counting board.

measurement speeds and high throughput analysis, adjustable repetition rates over orders of magnitude from the kHz to mid MHz regime allow for adapting the signal acquisition rates to the luminescence lifetime of the material.

In order to utilize the full range of capabilities offered by TRPL via TCSPC, the type of detector is essential for meeting the spectral and temporal criteria imposed by different semiconductor materials. Generally, the time scale of the respective charge carrier dynamics and spectral regime of the material specific photoluminescence dictate the necessary resolution and sensitivity of a detector. Four different detectors employed in this work are compared in their timing behavior and summarized in Table 3 with the relevant parameters. These include a red-sensitive photo multiplier tube (PMA-192, PicoQuant), two silicon-based SPAD-detectors (PDM-1CTC, Micro Photon Devices, and τ-SPAD, PicoQuant), and an InGaAs-based SPAD (SPD-A-M1, Aurea Technologies), which specifically allows for measurements up to 1700 nm. The PMT offers a compromise of intermediate time resolution down to a few hundred picoseconds and a reasonable sensitivity over the visible range up to 900 nm, while the best sensitivity (up to 75 %) is obtained with the single photon avalanche diodes (SPADs) at the cost of temporal resolution. In combination with picosecond pulsed excitation, the full range in time scales of charge carrier dynamics can be addressed, and luminescence lifetimes can be resolved with an instrument response function (IRF) down to 100 ps.

While the diode laser sources and the fast detectors for single photon counting constitute the basic components necessary for TRPL measurements, further instrumentation allows for expanding this purely time–domain technique. This is achieved with the use of spectrometers to resolve the characteristic emission bands within the total photoluminescence and general instrumentation to provide spatial resolution. The former is realized by integrating spectrometers typically employed for single photon emission counting and a fluorescence correlation spectrometer (FluoTime 300, PicoQuant) with a spectral resolution of 0.2 nm in the range of 200 to 1700 nm. Supplementing TRPL with spatial resolution is achieved with the full periphery required for lifetime imaging by a raster scanning microscope (MicroTime 100 and 200, LSM Upgrade Kit, PicoQuant). This periphery can be configured to cover lateral resolutions down to sub-micrometer scale and scan ranges from 80 μm up to several centimeters.

Results and Discussion. *Time-resolved photoluminescence spectroscopy (TRPL).* The central technique to characterize semiconductor systems via their charge carrier dynamics is time-resolved photoluminescence spectroscopy (TRPL) of the transient semiconductor emission [2, 3, 15]. In order to illustrate the principle of the approach, the picosecond laser diode emitting at 595 nm (LDH-P-FA-595, PicoQuant) to photoexcite a GaAsP quantum well system is employed in conjunction with the fluorescence spectrometer (FluoTime 300, PicoQuant). The time-resolved emission spectrum (TRES) in Fig. 1 acquired with the PMT detector (PMA-N-M-192) shows the photon statistics of the photoluminescence emission decay after photoexcitation in different spectral channels. Here, the capability of differentiating the charge carrier dynamics in the structural components that make up the GaAsP quantum well system is demonstrated by spectrally resolving the photoluminescence. The system is composed of the 10 nm GaAsP quantum well structure placed between two $Al_{0.4}Ga_{0.6}As$ barrier layers and deposited on a GaAs buffer layer. A thin GaInP etch-stop layer is introduced between the quantum well and the lower barrier. From a preliminary characterization of this system, the different spectral channels seen in Fig. 1 can be assigned. The peak at 652 nm is attributed to the AlGaAs barrier, the emission at 740 nm is from the GaAsP quantum well structure, and the emission at 860 nm stems from the GaAs layer and the substrate. Each emission channel in Fig. 1 shows a characteristic behavior with a complex multiexponential decay. This behavior can be analyzed according to the geometry and band structure of the GaAsP quantum well and the barrier and buffer layers that surround it. The analysis is not carried

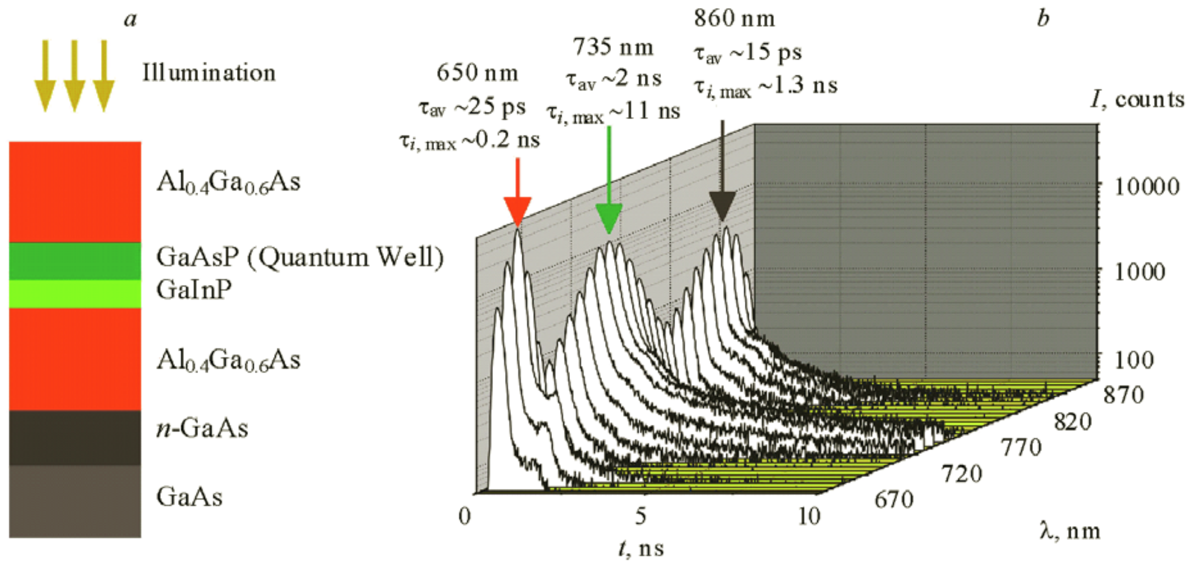

Fig. 1. Transient TRPL spectrum of a quantum well illuminated at 595 nm and measured with a FluoTime 300 spectrometer showing (a) the layer structure of the quantum well and (b) the time-resolved emission spectrum (TRES) of the wafer. The first peak at 650 nm stems from the $Al_{0.4}Ga_{0.6}As$-barrier, the peak around 735 nm from the GaAsP quantum well, and the peak around 860 nm from the *n*-GaAs layer and the GaAs substrate. Each spectral channel can be described with a three-component exponential model. The average lifetime and the longest component of the fits are displayed. The measurement exemplifies the correlation of characteristic charge carrier dynamics in material-specific spectral channels of the multi-component system.

out explicitly but the qualitative differentiation seen in Fig. 1 allows for the assignment of specific dynamics to a discrete architectural element of the system via the correlation to a characteristic emission band.

Multi-component excitation spectroscopy. In order to achieve a clear differentiation of the material components and their respective spectral contributions, the semiconductor emission can be recorded while scanning the photoexcitation over different excitation wavelengths. The technique is demonstrated with the GaAsP quantum well system. As shown in Fig. 2, the detection is chosen to match the prominent emission channels seen in the time-resolved photoluminescence of this system (Fig. 1). For detection at 650 and 740 nm, a gradual increase in the emission is seen in the excitation region from 450 nm up to approximately 600 nm for both detection channels. In the region of the band gap of the AlGaAs barrier, the drop in emission from the quantum well emitting at 740 nm correlates with an increase in the intensity of the substrate emission at approximately 860 nm. This behavior is attributed to the lack of absorption of the AlGaAs barrier layer below its band gap energy, which acts as a transmission edge and allows higher exposure levels and the corresponding enhanced emission from the buffer layer above 860 nm to be detected. This correlation of the excitation spectra in the region of the AlGaAs barrier band gap allows a specific spectral emission band in the photoluminescence lifetime measurement in Fig. 1 to be assigned unambiguously to the components of the semiconductor layer system, which is difficult to achieve with a pure time-domain approach or other measurement techniques.

Intensity-dependent photoluminescence spectroscopy. The injection levels of free charge carriers that result from different excitation intensities offer further insight into the system specific behavior of the charge carrier dynamics. Particular contributions to the charge carrier lifetime are intrinsically intensity dependent and can be differentiated from other contributions to the total charge carrier lifetime by varying the intensity in the photoexcitation [1]. This approach is demonstrated with the GaAsP quantum well system by using the picosecond laser diode (LDH-P-C-635B, PicoQuant) at 635 nm for excitation. To spatially limit the photoexcitation of the system to a defined area of approximately 100 μm in diameter, the measurements were performed using a microscope (MicroTime 100, PicoQuant). Figure 3 shows different emission lifetimes measured under excitation at 635 nm within a defined excitation area by a PDM-SPAD detector (MicroPhoton Devices) with a 664 nm long-pass edge filter.

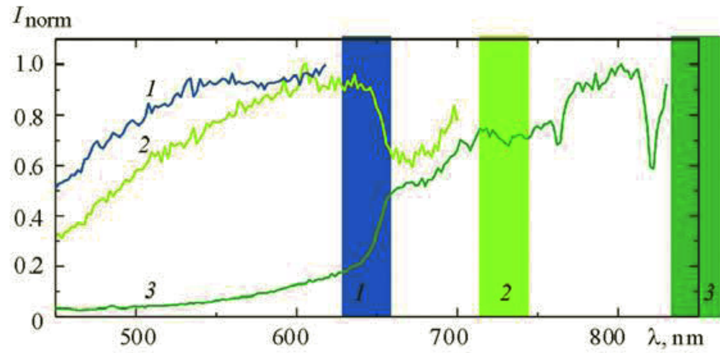

Fig. 2. Excitation spectra of the 650 nm peak of the $Al_{0.4}Ga_{0.6}As$ barrier (1), of the quantum well layer with the drop around 650 nm indicating the interaction with the barrier layer (2), and of the *n*-GaAs layer and GaAs substrate with the increase around 650 nm correlating with the absorption edge in the barrier at wavelengths longer than the barrier band gap (3). The rectangles illustrate the band gaps of the corresponding layers.

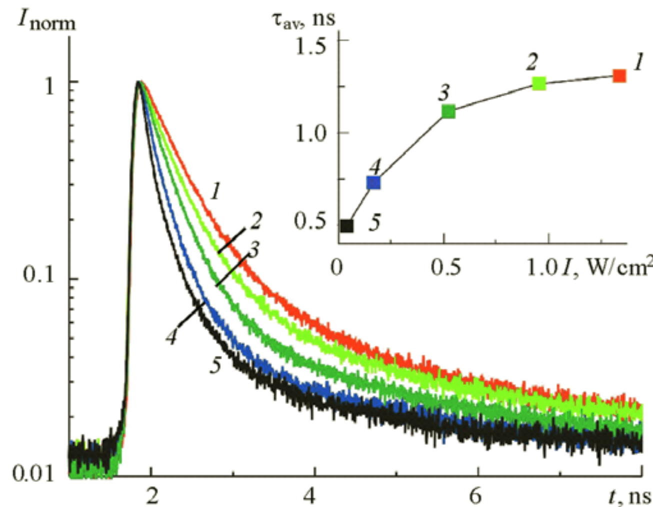

Fig. 3. Excitation intensity-dependent time-resolved photoluminescence of a GaAsP quantum well. The 635 nm diode laser was focused onto a 100 μm spot (FWHM) and the emission was separated using a 665 nm long-pass filter. The inset shows the saturation effect in the average lifetime obtained from the respective TRPL data curves 1–5 with the corresponding intensities as given in Table 4. The average lifetime approaches a fixed value, as expected, for high injection conditions in the Shockley–Read–Hall model of charge carrier recombination.

The recorded lifetimes can be fitted with a multi-exponential decay convoluted with the instrument response function. Using three components in the fit procedure with the values in Table 4 gives good agreement with the experimental data with the smallest number of components. In order to qualitatively illustrate the tendency of the global lifetime within the localized excitation area, the average value of the photoluminescence lifetimes is plotted as a function of the photoexcitation intensity. In this qualitative representation, the typical saturation behavior of the free charge carrier dynamics is evident in this high injection level regime. This aspect is critical for differentiating between various components of the charge carrier dynamics and allows for a correct modelling of the respective charge carrier lifetimes [1, 3, 19]. The intensity measurements given here can be seen as a prerequisite for the spatial mapping of charge carrier diffusion that will be given in the following subsections.

Lifetime Imaging Microscopy: carrier diffusion. With the understanding of localized charge carrier dynamics via its intensity dependence, phenomena of transport to specific regions of the semiconductor and circumstances that control

TABLE 4. Amplitudes and Time Constants for the Three-Component Model of Intensity-Dependent Photoluminescence Shown in Fig. 3

Intensity, W/cm^2	A_1	τ_1, ns	A_2	τ_2, ns	A_3	τ_3, ns	τ_{av}, ns	Number in Fig. 3
0.04	35200	0.08	855	0.56	231	2.48	0.49	*5*
0.17	29100	0.11	1210	0.62	221	3.44	0.73	*4*
0.52	22900	0.15	2070	0.66	306	4.19	1.12	*3*
0.96	19100	0.19	2920	0.73	376	4.35	1.27	*2*
1.34	17500	0.20	4179	0.73	457	4.2	1.31	*1*

charge carrier diffusion can be analyzed. This is achieved by combining time–resolved photoluminescence and lifetime imaging of the charge carrier dynamics. For this, the experiments are performed with the LSM Upgrade Kit mounted to the FluoView 1000 confocal microscope. The 440 nm picosecond laser diode is used to excite the GaAsP quantum well system. The photoluminescence emission is collected by scanning a detection area of approximately 1 μm in diameter on the sample surface while keeping the diffraction–limited illumination at a constant position. The photoluminescence is measured in a region of about 30 μm around the illumination site using a HQ735/50 nm bandpass filter and a SPAD detector (t-SPAD, PicoQuant). The acquired false color images of the photoluminescence lifetimes in the GaAsP quantum well are shown in Fig. 4. In order to address the spatial diffusion of free charge carriers, regions of interest (ROI) at increasing radial distances from the central point of excitation can be defined. At the point of excitation, the lifetime decays shown in Fig. 4 can be represented by a multi-component exponential decay model convoluted with the IRF. With increasing distance from the center of illumination, a rising component that exceeds the IRF has to be taken into account. This is expected for the temporal delay that is associated with the diffusion time over the distance determined by the point of excitation to the ROI. Here, both the spatial resolution offered by a diffraction limited illumination point and the short IRF are critical for resolving these dynamics. The contribution of charge carrier diffusion to the total photoluminescence lifetime is further illustrated by the shift in the rising edge of the photoluminescence intensity to longer delay times. The approach of scanning the detection volume over the semiconductor allows for an insight into the diffusion effects and their role in the general efficiency of semiconductor devices. This directly relates to charge carrier confinement and diffusion-mediated recombination dynamics that determine the threshold currents that this general multi-layer GaAsP–AlGaAs architecture provides in high power diode lasers [15–19]. For fully exploiting the capabilities of this technique, these measurements can be carried out in combination with spectral resolution of photoluminescence to characterize diffusion at and across material interfaces, and intensity dependent measurements to clearly differentiate the diffusion dynamics from other contributions to the charge carrier lifetime.

Lifetime imaging microscopy: spatial inhomogeneities. The aspects of charge carrier phenomena investigated above within the single crystalline GaAsP–AlGaAs system are primarily determined by the architecture of the layer structure and nature of the quantum well. The spatial inhomogeneity here is controlled and adjusted by the growth parameters, and microscopic morphology such as grain size does not play a role in this system. In order to fully demonstrate the capabilities available to the microscopic imaging of photoluminescence lifetimes in semiconductor systems, a multicrystalline CdTe–CdS heterojunction system is characterized in which post–deposition treatment results in a change in the grain size and general structural alterations that are central to the charge carrier dynamics and the respective efficiency of this system [5, 20–22]. The sample (3–4 μm CdTe; 200 nm CdS; 500 nm TCO on a glass substrate) is scanned with a MicroTime 200 confocal microscope (PicoQuant) using the picosecond laser diode at 635 nm for excitation. The surface mapping of the photoluminescence lifetimes is carried out before and after a post-deposition chloride activation process [20, 21]. Gray-scale intensity plots of the CdTe surface and false-color plots of the charge carrier lifetime are shown in Fig. 5. Also shown are the full statistics of the charge carrier lifetime over the scanned surface before and after the activation. Several key features of the data taken before and after the chemical treatment of the material give an insight into possible applications of this general approach. The gray-scale intensity images given for reference show the desired jump in emission efficiency resulting from the activation process. As shown in Fig. 5, the global change in the average photoluminescence lifetime from 0.27 to 0.60 ns is much more insightful for the analysis of the material and function of the system. This behavior documents the cause of the observed enhanced emission with the signature of a fundamental change in the general dynamics of charge carriers in

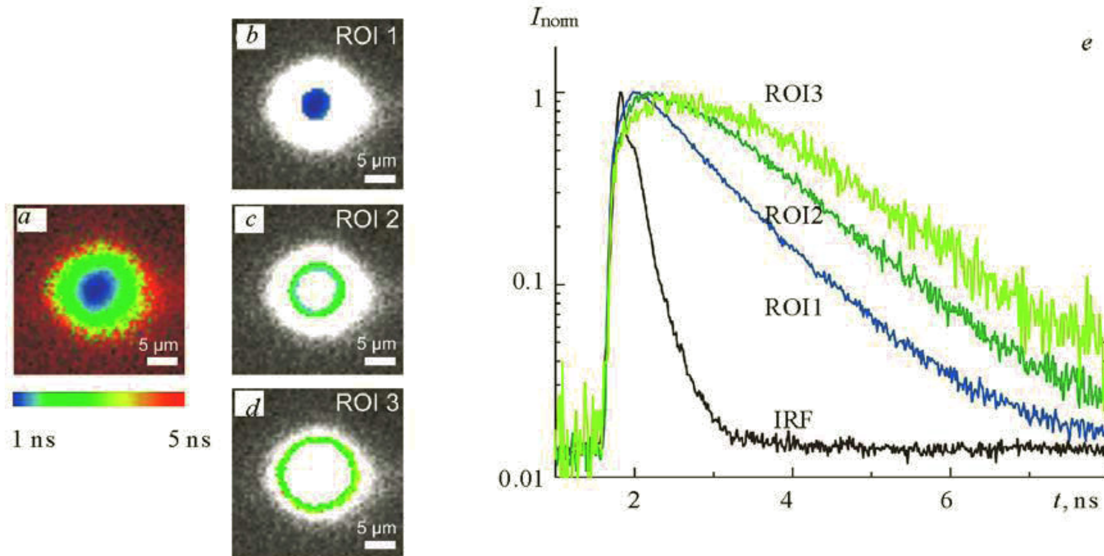

Figure 4. Carrier diffusion observed in a GaAsP quantum well system. The central spot of the image was illuminated with the 440 nm pulsed diode laser at 40 MHz, and the emission was filtered with the 735/50 nm bandpass filter. Only the detection volume was scanned over the image. The false color code in the different images of the ROI indicates that the average lifetime increases for larger radii from the point of illumination. This is shown with a complete lifetime mapping in (a) and individual ROI of increasing distance from the excitation in (b), (c), and (d). A closer look at the temporal behavior of the TRPL as shown in (e) reveals that the maximum in the transient photoluminescence shifts to later times with distance from the point of illumination. This is the result of the longer time scales for the charge carriers to migrate from the center of the image to the selected region of interest before emitting a photon from recombination. While the rise times vary, the primary decay component remains constant for around 1.1 ns. Only the center of the image shows a different behavior, where the decay is slightly shorter (roughly 1 ns) since diffusion from the point of excitation acts as an additional depleting component.

the material. Generally, chemical modifications that change the relative energies of acceptor and donor levels in the general band structure of the material can result in this global deceleration of the dynamics. A closer look at the false-color images of the spatial lifetime mapping in Fig. 5 reveals that the change in morphology correlates with this dramatic change in charge carrier dynamics. Additionally, the grain regions show a sharp contrast in photoluminescence lifetimes. Since the surface is oversampled, noise is ruled out as a source of these variations, clearly allowing further correlation of the morphology change induced by the chemical processing to the increase in emission intensity.

The results from spatial mapping of the photoluminescence lifetime before and after post–deposition chemical and thermal treatment are in good agreement with previous investigations of the mechanism underlying the enhanced efficiency of the CdTe–CdS multi-layer architecture [5, 20–22]. The effect has been directly correlated to both the crystallographic reorientation of the material and significant alterations in the grain size, although other effects can also play a role [20]. The spatially resolved photoluminescence measurements reaffirm these works via the global change in the charge carrier lifetime and its distribution within the altered grain structure of the material [22].

The above measurement scenarios for analysis of photoluminescence in semiconductor systems are all within the general instrumentation of TCSPC technology [14]. The repertoire of possible scenarios demonstrates the unique diversity of possible approaches to a complete and detailed analysis of the respective charge carrier dynamics. Importantly, the different aspects of charge carrier dynamics accessible with these techniques are intrinsically linked to the function, efficiency and quality of semiconductor devices and materials. The capability to address complex systems has been demonstrated with the

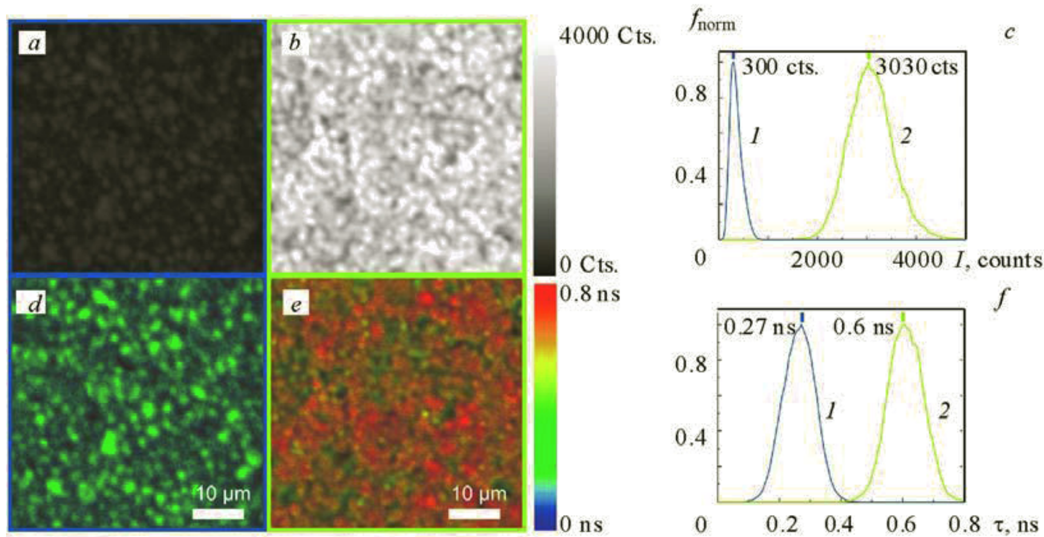

Fig. 5. A CdTe-polycrystalline wafer surface was scanned on a confocal microscope before and after thermal activation with a chloride compound. The respective intensity images (a) and (b) as well as the lifetime images (d) and (e) before and after treatment show a significant increase in intensity and photoluminescence lifetime after activation. The statistical distributions of the intensities (c) and lifetimes (f) over the full image are given before (1) and after (2) activation. With only a 3 ms/pixel measurement time, a distinctive change in the average lifetime can be observed as well as significant variations of the lifetime over different regions of the CdTe structure.

exemplary characterization of the single-crystal GaAsP quantum well and the multi-crystal CdTe heterojunction system [5, 15–22]. Importantly, the charge carrier dynamics and lifetimes in different components can be discriminated by spectrally and spatially resolving the photoluminescence, which allows for an evaluation of varying constellations in the architecture and morphology. For the GaAsP quantum well, spectrally resolved TRPL measurements in conjunction with excitation spectroscopy show the possibility to discriminate signals from different components and isolate the respective charge carrier dynamics types within a multi-layer system. This offers the possibility of analyzing the interfaces and cladding layers that surround the quantum well structure. Together with intensity-dependent measurements, imaging of photoluminescence in localized excitation regions further allows for a direct characterization of diffusion processes. In combination, these aspects are essential for understanding the phenomena of transport to specific regions of the semiconductor and the general conditions that control charge carrier migration when evaluating threshold currents and the general efficiency of high power GaAsP–AlGaAs laser diodes that utilize this architecture [15–19].

The measurement principles demonstrated on the GaAsP quantum well system are equally relevant for the multi-layer CdSe–CdTe heterojunction. The interfusion of sulfur and tellurium and moderate spectral shifts due to post-deposition treatment that allow for the transition from a *p–i–n* to true *p–n* heterojunction can also be accessed with the spectrally resolved measurements used for the GaAsP system and this effect can be evaluated in the context of the associated change in the charge carrier lifetime [21–23]. In this work, the CdTe system provides for the opportunity to address varying charge carrier dynamics in microscopic structures. Generally, the post-deposition treatment of the CdTe system and the resulting grain alteration can be directly correlated to a change in the global photoluminescence lifetime. Since the measurements are preformed using lifetime imaging microscopy, the spatial distribution of photoluminescence lifetimes can be associated with changes in grain dimensions before and after treatment. So, the charge carrier dynamics provide a direct link between microscopic morphology and the mechanism behind the change in the efficiency of the system.

Conclusions. In summary, the multi-dimensional approach of TRPL via TCSPC can be seen as a technique highly suitable for a sensitive and precise characterization of a particular semiconductor system. Future developments in this general methodology can include spectrally resolved lifetime mapping and the simultaneous acquisition of reflectance images to

enhance the information gained from morphology specific imaging. Due to the versatility of the approach, the field of possible applications is expected to range from the fundamental research of semiconductor systems and the engineering of specific devices to the mapping of wafers in industrial material research and process control.

REFERENCES

1. S. M. Sze and K. K. Ng, *Physics of Semiconductor Devices*, 3rd ed., New Jersey, Wiley (2007).
2. R. K. Ahrenkiel, N. Calla, S. W. Johnston, and W. K. Metzger, *Sol. Energy Mater. Sol. Cells*, **94**, 2197–2204 (2010).
3. S. Rein, *Lifetime Spectroscopy: A Method of Defect Characterization in Silicon for Photovoltaic Applications*, Springer Series in Materials Science, Berlin, Springer (2010).
4. P. V. Santos, F. Alsina, S. K. Zhang, R. Hey, A. García-Cristóbal, and A. Cantarero, *Physica E*, **13**, 467–472 (2002).
5. W. K. Metzger, D. Albin, D. Levin, P. Sheldon, X. Li, B. M. Keyes, and R. K. Ahrenkiel, *J. Appl. Phys.* **94**, 3549–3555 (2003).
6. D. A. Bender, M. P. Hasselbeck, and M. Sheik-Bahae, *Proc. SPIE Int. Soc. Opt. Eng.*, **6461**, 646109 (2007).
7. B. M. Keyes, P. Dippo, W. K. Metzger, J. AbuSchama, and R. Noufi, *J. Appl. Phys*. **94**, 5584–5591 (2003).
8. H.-M. Cheng and F.-W. Hsieh, *Nanotechnology*, **21**, 485202 (2010).
9. A. Douhal, C. Martin, M. Ziolek, and M. J. Marchena, *J. Phys. Chem. C*, **115**, 23183–23191 (2011).
10. H.-J. Huang, F.-C. Chien, P. Chen, K.-C. Ho, and C.-W. Chu, *Anal. Chem.*, **82**, 01669–01673 (2010).
11. J.-L. Wu, F.-C. Chen, Y.-S. Hsiao, F.-C. Chien, P. Chen, C.-H. Kuo, M. H. Huang, and C.-S. Hsu, *Nano*, **5**, 959–967 (2011).
12. S. Itzhakov, S. Buhbut, E. Tauber, T. Geiger, A. Zaban, and D. Oron, *Adv. Energy Mater.*, **1**, 626–633 (2011).
13. Z. Bian, T. Tachikawa, S.-C. Cui, M. Fujitsuka, and T. Majima, *Chem. Sci.*, **3**, 0370–0379 (2012).
14. W. Becker, *Advanced Time-Correlated Single Photon Counting Techniques*, Springer Series in Chemical Physics, Berlin, Springer (2005).
15. G. Erbert, F. Bugge, A. Knauer, J. Sebastian, A. Thies, H. Wenzel, M. Weyers, and G. Tränkle, *IEEE J. Sel. Top. Quantum Electron.*, **5**, 780 (1999).
16. H. Wenzel, G. Erbert, F. Bugge, A. Knauer, J. Maege, J. Sebastian, R. Staske, K. Vogel, and G. Tränkle, *Proc. SPIE Int. Soc. Opt. Eng.*, **3947**, *32–39* (2000).
17. A. Knauer, F. Bugge, G. Erbert, H. Wenzel, K. Vogel, U. Zeimer, and M. Weyers, *J. Electron. Mater.*, **29**, 53–56 (2000).
18. P. Crump, H. Wenzel, G. Erbert, P. Ressel, M. Zorn, F. Bugge, S. Einfeldt, R. Staske, U. Zeimer, A. Pietrzak, and G. Tränkle, *IEEE Photonics Technol. Lett.*, **20**, 1378–1380 (2008).
19. J. Sebastian, G. Beister, F. Bugge, F. Buhrandt, G. Erbert, H. G. Hänsel, R. Hülsewede, A. Knauer, W. Pittroff, R. Staske, M. Schröder, H. Wenzel, M. Weyers, and G. Tränkle, *IEEE J. Sel. Top. Quantum Electron.*, **7**, 334–339 (2001).
20. M. Hädrich, H. Metzner, U. Reislöhner, and C. Kraft, *Sol. Energy Mater. Sol. Cells*, **95**, 887–893 (2011).
21. B.E. McCandless and R.W. Birkmire, *Solar Cells*, **31**, 527–535 (1991).
22. W. K. Metzner, D. Albin, M. J. Romero, P. Dippo, and M. Young, *J. Appl. Phys*., **99**, 103703 (2006).
23. V. Yu. Timoshenko, A.B. Petrenko, M. N. Stolyarov, T. Dittrich, W. Fuessel, and J. Rappich, *J. Appl. Phys*., **85**, 4171–4175 (1999).
24. M. Roczen, E. Malguth, M. Schade, A. Schöpke, A. Laades, M. Blech, O. Gref, T. Barthel, J. A. Töfflinger, M. Schmidt, H. S. Leipner, L. Korte, and B. Rech, *J. Non-Cryst. Sol*., **358**, 2253–2256 (2012)